JATIS Journal of Astronomical Telescopes, Instruments, and Systems

RESEARCH PAPER

Convolutional neural network design for the prediction of the focusing temperature of PLATO telescopes under simulated space operating conditions

Guillermo Mercant Rubio,[a,*] **Gonzalo Ramos Zapata**,[b] **José Ramón Rodón Ortiz**,[c] **Jesús Saiz**,[d] **Nicolas Gorius**,[e] **Bart Vandenbussche**,[f] **Martin Pertenais**,[g] **Jose Lorenzo Alvarez**,[h] **and Miguel Mas**[a]

[a]Centro de Astrobiología (CAB) CSIC-INTA, Torrejón de Ardoz, Spain
[b]INTA, Instituto Nacional de Técnica Aeroespacial, Torrejón de Ardoz, Spain
[c]Instituto de Astrofísica de Andalucía (IAA-CSIC), Granada, Spain
[d]BLASAI, Cuenca, Spain
[e]INAF, Osservatorio Astrofisico di Catania, Catania, Italy
[f]KU Leuven, KUL, Institute of Astronomy, Leuven, Belgium
[g]Institute of Optical Sensor Systems, German Aerospace Center, DLR, Berlin, Germany
[h]ESA, European Space Agency, Noordwijk, The Netherlands

ABSTRACT. The main science goal of the PLAnetary Transits and Oscillations of stars mission is to detect and characterize extrasolar planets around solar-type stars. For this purpose, the telescopes developed for the mission have a focusing system consisting on to tune the thermal surrounding of the opto-mechanics for achieving the optimal focus. We propose an alternative method for determining the best focus temperature. We designed a convolutional neural network that uses images obtained in ground performance evaluation to implement a calibration method to be used during pre-launch tests and orbital tuning. The convolutional neural network effectively predicts focusing temperatures, improving calibration efficiency and accuracy. This approach demonstrates the potential of artificial intelligence methods for optimizing telescope focusing in operational conditions.

 [DOI: 10.1117/1.JATIS.12.1.018005]

Keywords: PLAnetary Transits and Oscillations of stars; exoplanets; convolutional neural networks; space instrumentation; telescope calibration

Paper 250151 received Sep. 24, 2025; revised Feb. 6, 2026; accepted Feb. 9, 2026; published Feb. 26, 2026.

1 Introduction

The PLAnetary Transits and Oscillations of stars (PLATO)[1] mission is the third medium-class mission of the European Space Agency (ESA) Cosmic Vision program.[2] It is composed of 26 telescopes with the objective of detecting and characterizing Earth-like exoplanets in the habitable zone of solar-type stars. The mission is scheduled to be launched in 2026 and will be located at the $L2$ Lagrange point between the Earth and the Sun.[3]

PLATO's cameras are designed to detect tiny variations in the brightness of stars caused by planetary transits, both primary and secondary, within a wide field of view. One of the main technological challenges of the project is the ability to detect and quantify small fluctuations in the brightness of the millions of stars covered by the large number of images.

*Address all correspondence to G. Mercant, gmercant@cab.inta-csic.es

Each of the 26 telescopes that will be part of the satellite is equipped with a focusing system that uses variations in temperature to achieve the highest quality images, without the need for active focusing mechanisms. Focusing is adjusted through the thermal contraction or expansion of the materials that make up the telescope structure, positioning the image in the best focus plane, where both the best size and energy of the point spread function (PSF) are obtained.

One of the objectives during the thermo-vacuum tests carried out at the facilities of the National Institute for Aerospace Techniques (INTA), together with the other two institutions involved in these activities (IAS and SRON), is to determine the optimal focusing temperature for each of the cameras that make up the telescope. To do this, the system's environmental conditions of pressure and temperature are simulated, and the quality of the images is analyzed for different temperatures.

During the lifetime of the mission, a daily data volume of 435 Gb of images is foreseen, which has to be transmitted, stored, and processed. These data have to be processed both on the instrument and on the ground, so a tool that allows data processing while reducing the amount of data is very useful.[2]

Numerous missions dedicate part or all of their lives to the search for exoplanets, such as the Kepler, James Webb, TESS, and the future ARIEL missions, and among others, to the detection of transient[4] events such as those that PLATO aims to observe, so the availability of the data for facilitating the synergies should be considered even more important.

This work presents an application of convolutional neural networks (CNNs) in the field of astronomy, where the feature extraction techniques through image processing have been applied to a variety of applications,[5] from galaxy classification[6] to image denoising.

The main objective of this work is to develop an alternative method for obtaining the focusing temperature of the PLATO space telescope cameras. To this end, we propose the design of a CNN which, through the experimental images obtained by means of the thermal vacuum tests prior to the launch of the mission, is capable, in the event of demonstrating correct operation during the ground tests, of providing an accurate prediction method in the orbital calibration process using the first images captured by the telescope.

2 Space Operational Conditions

To understand the origin and features of the images, a general description of the operational space conditions is mimicked during the on-ground calibration and characterization testing campaign. To briefly explain such performance evaluation tests, the environmental conditions of the tests, the parameters to be monitored, and the configuration of the telescopes for acquisition of images together with the type of data obtained are described.

As previously pointed out, the main objective of the PLATO space mission is to detect terrestrial exoplanets around solar-type stars. To achieve this goal, the sensitivity of the detection systems needs to be able to identify minimal variations in the brightness of these stars. PLATO space observatory consists of a set of 26 telescopes that have to be characterized and verified under operational conditions for ensuring the achievement of the scientific goals of the mission.[7] Each telescope is equipped with an optical system supported by a structure called Telescope Optical Unit, a proximity electronics front-end electronics and a structure forming its own focal plane and focal plane assembly (FPA) containing four charge-coupled device (CCD) image sensors of 4510×4510 pixels each in the case of the 24 N-type cameras available (Fig. 1).

2.1 Optical Fundamentals

The physical principle behind the thermal focusing system that PLATO telescopes are equipped with is to control the temperature of both the optical components and the structural elements of the system. By thermal contraction and expansion of the opto-mechanical elements, the distance between the optical elements and the camera sensor is controlled, allowing the focal length of the system to be adjusted and optimal focusing of the images to be achieved.[8]

The focusing system can adjust the temperature of the optical and/or opto-mechanical components using electronically controlled heating devices. These devices allow precise temperature tuning which is translated into the corresponding focal length adjustment needed for achieving the desired focused images.

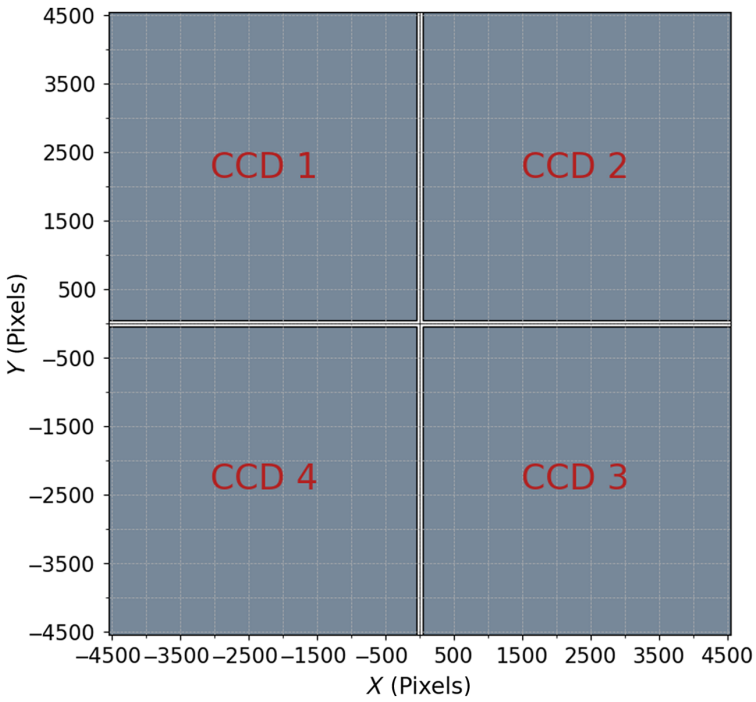

Fig. 1 Focal plane of the N-type telescope formed by four full-frame CCDs of 4510 × 4510 pixels each.

The quality of an optical system can be assessed using the PSF, which describes how the system—specifically, the telescope's lens system—scatters light from a distant point source, assuming collimated transmission upon incidence on the telescope.[9]

In this case, to determine the best focus temperature (BFT) of each telescope, a statistical analysis of the energy that is concentrated in the images that the cameras form when illuminated with a collimated beam of light is performed for each temperature, obtaining the temperature at which the energy is concentrated in the minimum area.

Experimentally, the quality of a system's PSF can be approximated using the ensquared energy fraction (EEF), which quantifies the fraction of total energy concentrated within a specific area around the image of a point source in the focal plane, relative to the total energy of that image.[10] This measure provides insight into the system's efficiency, as the PSF and EEF are directly related (Fig. 2).

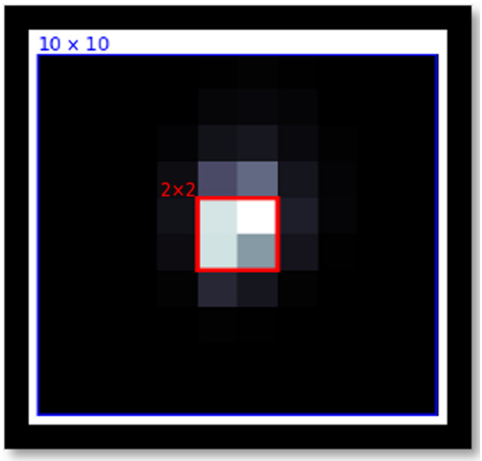

Fig. 2 Example of an image with 58.8% EEF and approximate representation of its PSF.

The core of the analysis in this work consists of the calculation of the EEF for each image, which is defined, in this case, as the fraction of energy concentrated in 2×2 squared pixels in a 10×10 squared pixel area. To calculate it, the brightest pixel is identified, and the 2×2 square containing the highest energy is plotted around it. The next step is to compare the sum of the values of these 4 pixels with the total energy of the PSF considered mostly contained in 10×10 px^2, as verified during the instrument design phase. If a very large surrounding area is considered, the noise values of the image would be included in the calculation, whereas if a too small an area is considered, the values related to the way the optical system distributes the energy due to its intrinsic characteristics would be omitted. Therefore, given that the size of the PSF in the conditions of greatest defocus does not exceed the size of 10×10 pixels, this area value is set to include all the relevant PSF signal. From this, the EEF is calculated as follows [Eq. (1)]:

$$\mathrm{EEF}(2 \times 2 \text{ mm}) = \frac{\sum \mathrm{Energy}_{\mathrm{area2\times2}}}{\sum \mathrm{Energy}_{\mathrm{area10\times10}}} = \frac{\mathrm{EE}_{2\times2}}{\mathrm{EE}_{10\times10}}. \tag{1}$$

Due to the characteristics of the optical design, the best focusing temperature of each telescope will correspond to the position where the EEF is uniform along the focal plane, for which the average EEF of all field positions is highest.

2.2 Test Setup

The thermo-vacuum test configurations described in this section were defined during earlier opto-mechanical and system-level design phases of the PLATO space telescope, which are outside the scope of this paper. In the present work, we make use of the available test data and configurations as provided, focusing on the analysis and exploitation of the acquired images for focus temperature estimation rather than on the definition or optimization of the test parameters themselves.

The data for this work have been obtained from the thermo-vacuum tests carried out at INTA during the verification and calibration under operational conditions of the engineering model (EM) and the first flight models (FMs) of the PLATO space telescopes. To date, one EM and three flight models, FM3, FM6, and FM10, have been tested, and the data for the analysis and design of the neural network are available. A complete description of the test setup and all the performance tests carried out for the different models is provided elsewhere.[11,12]

This paper focuses on one of the main objectives of functional testing under PLATO operating conditions, which is to determine the temperature at which the optimum focus is obtained. For this purpose, a thermal profile is performed (Fig. 3), which consists of simulating the

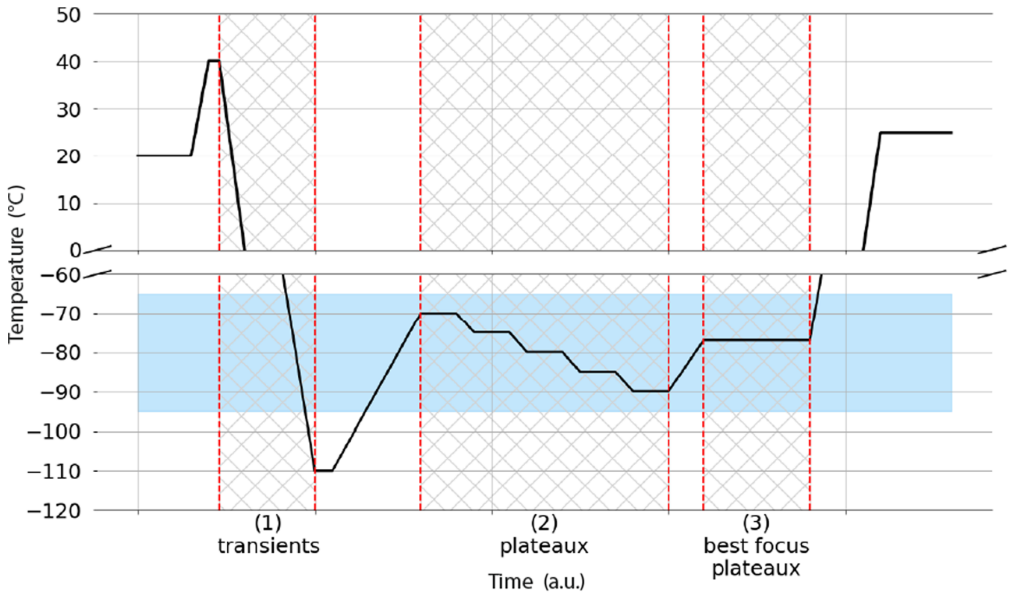

Fig. 3 Thermal profile of the test divided into three regions: (1) transients, (2) best focus search plateaux, and (3) best focus plateau.

operating conditions of pressure and temperature in which the instrument will experiment during its flight and, finally, in which it will operate. This process allows the validation of the different components of the system, also allowing the characterization on the ground of each of the telescopes included in the mission.

Figure 3 shows the thermal profile to which each telescope is subjected as soon as a vacuum level of 10^{-5} mbar or lower is reached. For the application of this study, the thermal profile can be divided into three distinct regions: transients (1), plateaux for the best focus temperature determination (2), and best focus plateau (3). The blue band corresponds to the operating temperature region, between −65°C and −95°C.

In the first region, corresponding to the transient measurements, the temperature of the optical system is gradually modified, and continuous image acquisition is performed. During the period of time that the telescope is in this region, the thermal stability of the system is not ensured, so the images acquired in these positions are not included in this study.

At the second region, the best focus search plateaux, the images are acquired in five discrete temperature regions, corresponding to temperatures of −90°C, −85°C, −80°C, −75°C, and −70°C at which the telescopes are stabilized. During these acquisitions, thermal stability of the system is ensured by maintaining conditions within a temperature acceptance range of no more than ±0.1°C for a set of the telescope thermal sensors, basically those involved in the temperature tuning for finding the best focus.

Finally, in the best focus plateau region, image acquisition is performed with the telescope stabilized at the best focus temperature determined by polynomial regression from the results obtained in the previous phase. For this, the maximum EEF is calculated for each field of view (FoV) and for each temperature plateau. Then, the polynomial adjustment is performed, the maximum of which corresponds to the temperature of best focus, the temperature at which the EEF is maximum.

Before an observation starts, the parameters with which the test will be carried out are configured, including the exposure time of the image, the field positions, and the number of frames. Once the parameters have been defined, the images and telemetry measurements of the optical system and the monitoring systems of the installations are obtained during the established time, thus making up a complete observation.

Figure 4 shows the sequence of the CCD's path for image acquisition used in the framework of the PSF characterization test at the nominal best focus temperature run for each PLATO telescope. It shows the locations corresponding to the four CCDs and the different field positions where the images are formed. In this test configuration, 40 different field positions are established for characterization, which allows the distribution of the images and their quality and EEF to be studied along the entire detection plane.

The optical defocusing of the telescope at temperatures far away from the best focus temperature results in a significant difference among the images corresponding to central positions of the field (images obtained in "on-axis" configuration) and those farther away from the optical axis of the telescope (theoretical center of its detection stage) (Fig. 5), which leads to a larger variation in the EEF of the images at that temperature.

3 Methodology

In this work, we propose an alternative method to determine the focusing temperature by applying a CNN through the experimental data obtained on ground thermo-vacuum tests. Taking advantage of the images acquired during these test campaigns, the proposed approach aims to extract the maximum amount of information achievable with the instrument's current optical design, without introducing additional optical elements or modifications to the nominal configuration. For this purpose, the images obtained during the observations are first preprocessed. Then, to establish a reference and be able to compare the results obtained, the focusing temperature is calculated by means of an interpolation. Finally, we proceed to the design, training, and implementation of the convolutional neural network, analyzing the results obtained and comparing them with those obtained mathematically.

The structure of the general development can be summarized as follows.

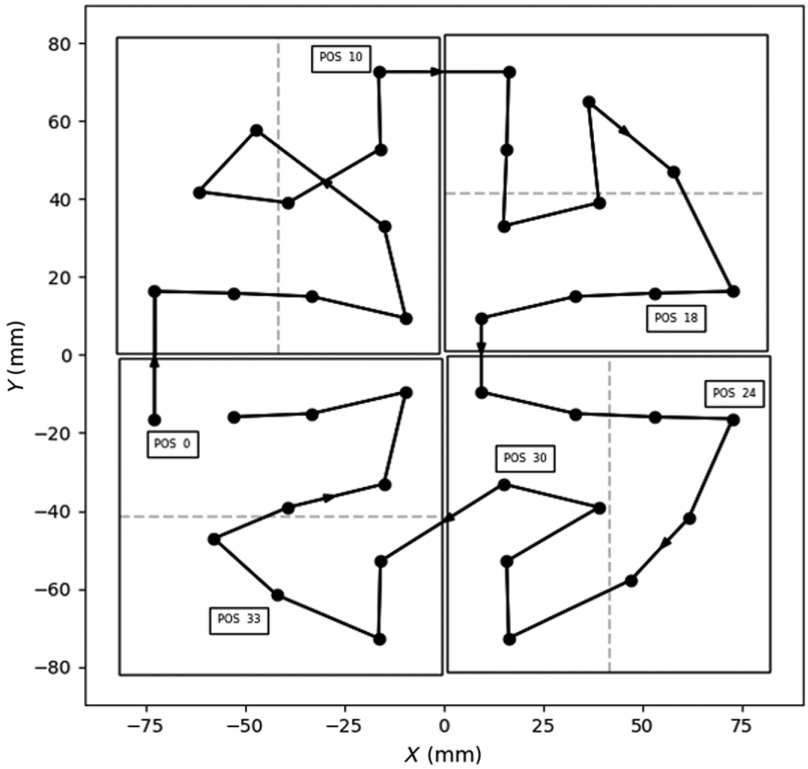

Fig 4 Forty FoV positions for the established test configuration.

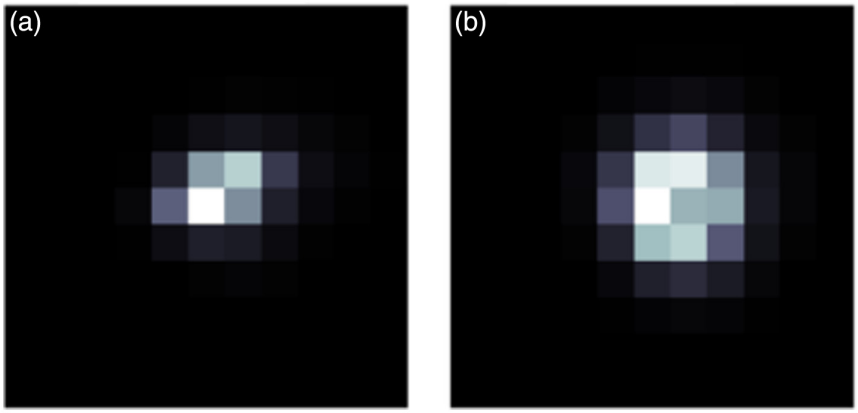

Fig. 5 Example of images in different field position at $T = -70°$ of the FM3 model. Image in a central position (a) and an off-axis position (b).

Initially, a detailed description of the structure and origin of the data available for the study is made. Once the structure and origin of the data are known, the data are reduced. To do this, the variables that are not correlated with the established objective are eliminated, the amount of information stored in the images is reduced, and the spatial size of the images is reduced around the pixel of greatest intensity. For the processing of the images, they are labeled with the temperature of the system at which the image was taken, and the calculation of the EEF corresponding to each of them is included.

With the images labeled and prepared for processing, the best focus temperatures of each model are calculated, using this as a reference for the comparison of the results obtained in the neural network. To calculate the focusing temperature, a non-linear regression of the EEF with the temperature is performed, so the maximum of the fitting curve corresponds to the best focusing temperature for the model under analysis.

Once the target temperature of each model is available, the design of the neural network is ready to be initiated. The design of the neural network is carried out progressively, being the first neural network model capable of making a classification or simple regression task to make adjustments to the network parameters and study the behavior of the network. The final proposed design is able to predict the focus temperature for each image processed through the developed CNN.

Finally, the CNN predictions are evaluated in the form of probability distributions for each chamber model. The temperature values are obtained and compared with those predicted by the polynomial fit, evaluating the accuracy and error metrics obtained.

3.1 Image Pre-Processing

As the telemetry data acquisition system is defined in a generic way for all types of tests, variables corresponding to redundant sensors, registers indicating the sensor status (on or off), and null values are discarded. From 165 monitoring variables, the matrix is reduced to 20 variables, and by carrying out the correlation matrix of the resulting variables, the sensor that determines the reference temperature of the telescope during the tests is established together with the time record to have a traceability of the data and its origin.

3.1.1 *Reduction of telemetry data*

For a successful implementation of the neural network, it is necessary to carry out a previous image processing. The objective of the data pre-processing is to extract the necessary knowledge from the images to efficiently design the convolutional neural network. The pre-processing task consists of reducing the data from the sensors and monitoring system, removing the background from each image and labeling the images, and reducing the spatial dimensions of the images to a manageable size.

3.1.2 *Background removal from each image*

To have a reference of the noise generated in the CCD sensors of the camera, background images are taken between each acquisition during each test. For a correct treatment of the images, the background noise must be subtracted from each image. To do this, the matrix subtraction of each image value by the value of the background obtained in the previous acquisition is carried out. This process reduces by half the number of images that are stored for processing, as the resulting images have already undergone noise reduction.

3.1.3 *Spatial image size reduction*

In the case of the full-frame detectors (i.e., for the N or "normal" type cameras), the size of each CCD is 4510×4510 squared pixels, and each camera consists of four CCDs. As the relevant size of the PSF under operational conditions is never larger than $\sim 10 \times 10$ squared pixels, the rest of the image is basically noise. The images are reduced in size to 10×10 arrays around the brightest pixel, the size established for the EEF calculation, resulting in a considerable reduction of the data to be processed.

3.1.4 *Labeling of the images*

For the correct processing of the images, it is necessary to associate each image with its acquisition temperature. For this purpose, after reducing the telemetry data, the temperature variable is assigned to each image. To do this, the image data files, stored in the Flexible Image Transport System format, which contain the time record of each image acquisition, are cross-correlated with the telemetry data, allowing the temperature associated with each image to be retrieved.

3.1.5 *Image normalization*

Image normalization is a common practice in CNN image processing.[13] The results obtained using image normalization have been explored, but normally, such results are conditioned by the normalization used for each model, producing incorrect image prediction. For this activity, the images have not been normalized, because the variability of the maximum intensity values in each of the images does not allow the establishment of a valid normalization criterion common to all the models.

For this reason, it was decided to design the network with the intensity values of the real images, allowing the model to be applied generically to all the images taken and to be taken in the future.

3.2 Statistical Determination of the Focusing Temperature

Determining the best focus temperature of each telescope tested is one of the first steps in calibrating the PLATO telescopes. A key requirement for determining the best focus temperature is to achieve an accuracy of ±3°C during ground characterization. This temperature will be further fine-tuned during the on-orbit recalibration phase as part of the mission commissioning process.

To determine the best focus temperature, the EEF is plotted as a function of temperature. The EEF depends on the FoV in which the image has been generated, so the energy depends on the radial distance to the center of the photosensitive sensor element, in this case, the array of four CCDs that make up the FPA.

As the calculation of the focusing temperature with this method involves considering each of the FOVs to make the adjustment, no distinction will be made among the images per FOV. Subsequently, with the calculation of the focusing temperature by means of the neural network prediction, the dependence of the BFT calculation on the field position will be studied. For this purpose, a single fourth-degree polynomial adjustment is made for each plateau, without distinguishing between the position at which the image was taken within the CCD (Fig. 6). The residual graph of this figure represents the difference among the BFT values interpolated using polynomial fitting and the BFT values obtained experimentally for each temperature plateau.

For each of the five temperature plateaux, the average of the maximum EEF values is calculated at each field of view position. This process involves determining the maximum EEF value at each field of view position from the images taken at various field positions. Then, the average of these maximum values is calculated for each field of view, thus obtaining the average value of all field of view positions for each temperature.

Once the mean EEF values are obtained for each temperature, they are plotted as shown in Fig. 7 and fitted to a fourth-degree polynomial. The maximum value of this polynomial corresponds to the maximum value of the EEF, which indicates the optimum focusing temperature for that telescope model under evaluation.[14]

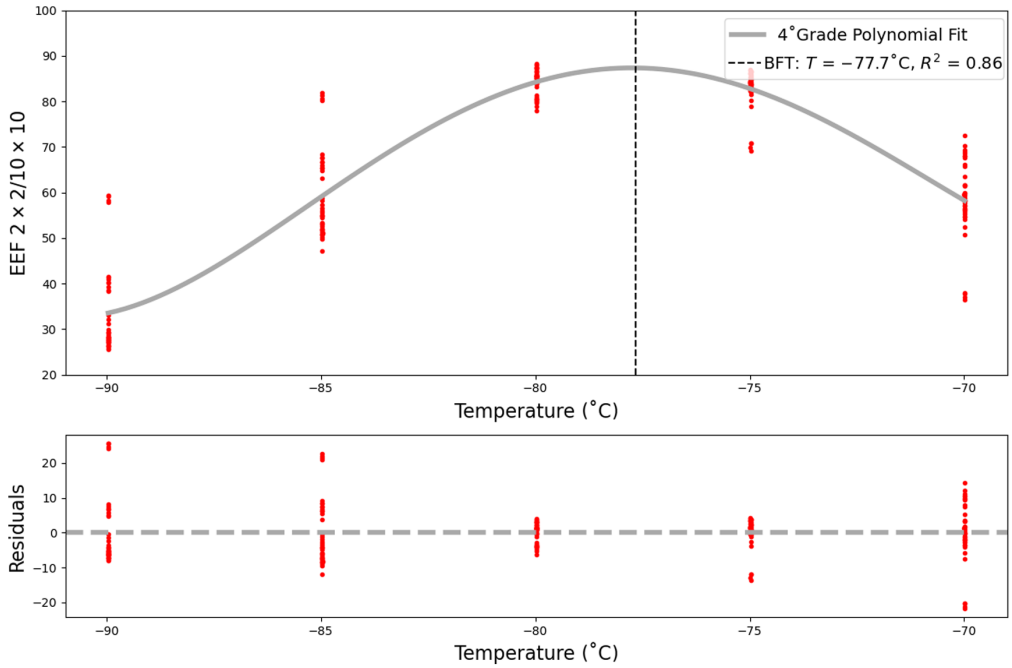

Fig. 6 BFT estimation for the FM3 model using a single fourth-degree polynomial fit for all field positions.

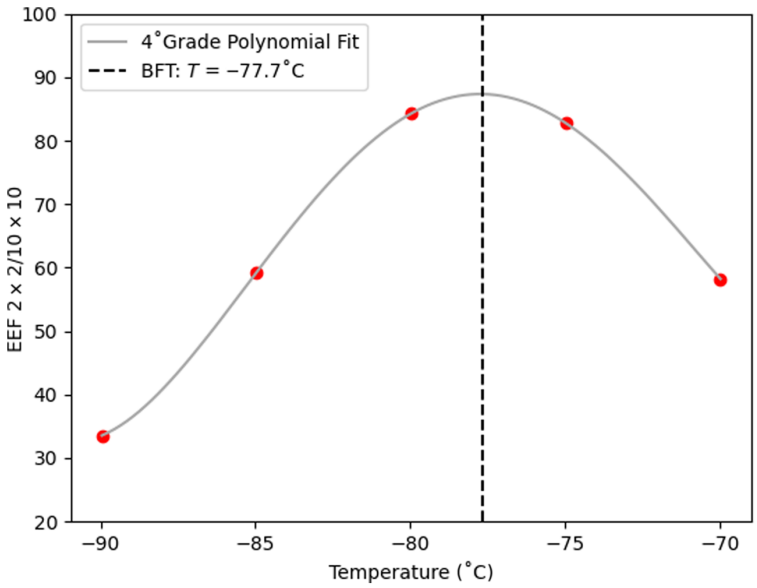

Fig. 7 BFT estimation of the FM3 model. Polynomial fourth-degree adjustment of the mean EEF value by plateau.

Figure 8 below plots the energy distribution, EEF, as a function of field for different temperatures. This visualization allows us to detect manufacturing anomalies and to observe the characteristic "hat shape" that PLATO's telescope design produces when plotting the EEF with the field.

Using this representation, once the best focus temperature is reached at the telescope (particularly, −77.7°C for FM3), the energy distribution becomes uniform over the entire detection surface, as can be observed in Fig. 9.

Using this method, the focusing temperatures for each model tested are obtained as summarized in Table 1, together with the estimated maximum EEF for the focusing temperature.

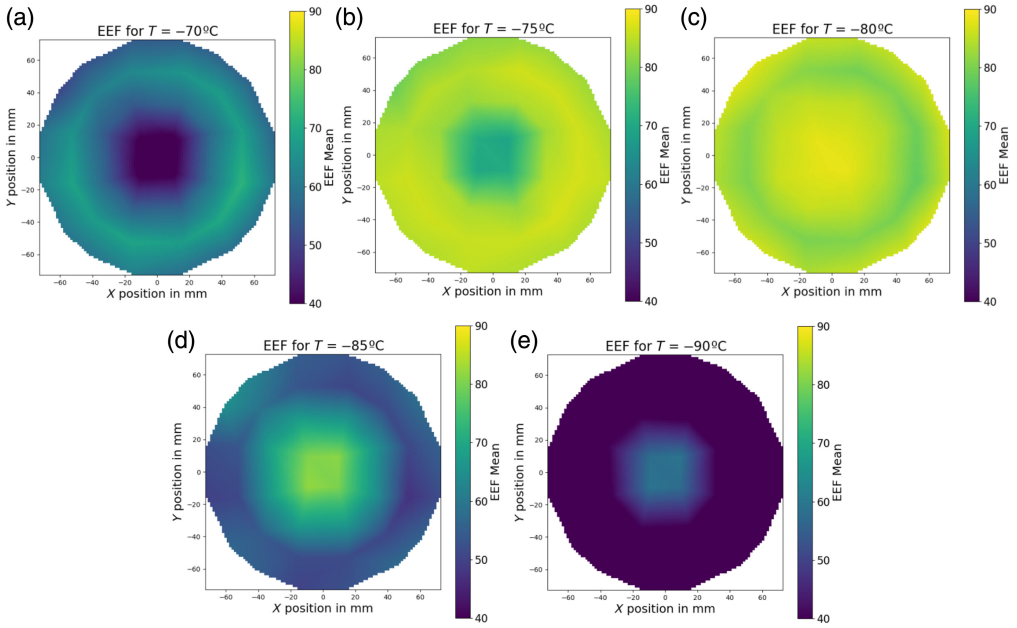

Fig. 8 EEF for each temperature plateau. (a) $T = -70°C$. (b) $T = -75°C$. (c) $T = -80°C$. (d) $T = -85°C$. (e) $T = -90°C$. Model FM3.

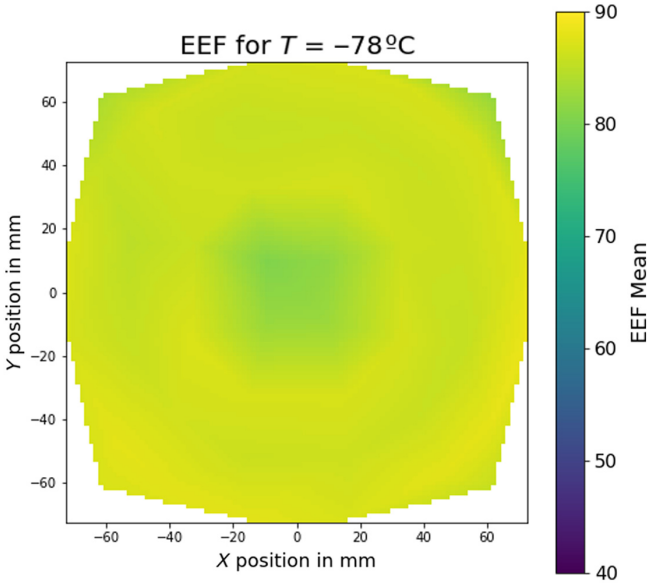

Fig. 9 EEF of the best focusing plateau. Model FM3.

Table 1 Summary of temperatures for best focusing and energies by model.

Model	BFT (°C)	Max. EEF (%)
EM	−75.7	79.9
FM3	−77.7	87.3
FM6	−80.1	87.0
FM10	−82.8	86.5

3.3 CNN Design

The main goal of implementing a convolutional neural network is to determine the optimal focusing temperature for each flight model of the PLATO telescope. To achieve this goal, the implementation of the convolutional neural network is carried out sequentially, starting the process with simpler design architectures and increasing the complexity of the system gradually. The first neural network model is designed with the purpose of predicting the temperature of the images corresponding to the five temperature plateaux, classifying them in the possible temperature ranges for the FM3 flight model. The design of this network seeks to establish a common structure for the rest of the designs, adjusting the network parameters appropriately, and the first network design is proposed as shown in Fig. 10.

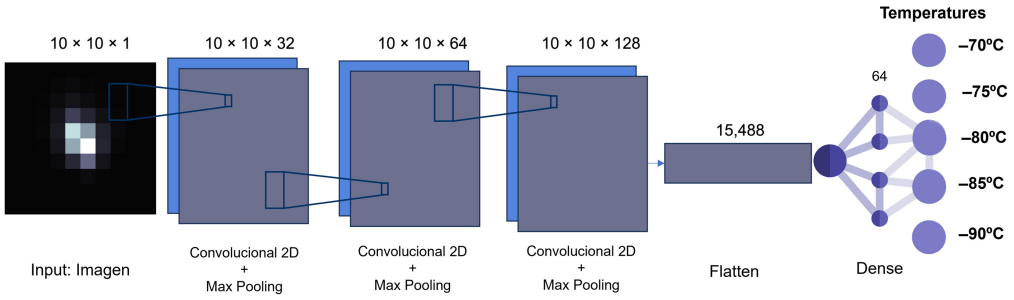

Fig. 10 Proposed neural network architecture.

The proposed neural network architecture is designed to analyze input images of size 10×10, in a single channel representing the intensity scale of the image. It consists of three successive convolutional layers of 32, 64, and 128 filters, each followed by a maximum pooling layer (MaxPooling2D) with a pooling size of (1, 1). The convolution layers use the rectified linear unit (ReLU) activation function and have padding to maintain the dimensions of the input features. At the output of the network is a flattening layer, which converts the output into a one-dimensional vector, followed by 2 dense layers, one with 64 units and ReLU activation, and another output layer with 5 units and softmax activation, to classify the images into one of the five temperature categories.[15]

Due to the classification nature of the network, sparse categorical cross-entropy is used as a training loss function and accuracy as an evaluation metric.[13] By means of this design proposal, the prediction of the temperature of the images of the plateaux is carried out, obtaining the results shown in Fig. 11, represented by a confusion matrix, which indicates the differences between the predicted and real temperatures. The accuracy of the classification of the images can be verified, as it correctly classifies ~99% of the images of the plateaux.

In the following, the design of a network that performs a prediction on the EEF of each of the images is proposed. For this purpose, the same CNN structure is used, modifying the output by a single unit, which allows the EEF value to be obtained, and modifying the loss function by MSE and the evaluation metric by the mean absolute error. As can be seen in Fig. 12, the real values and the values predicted by the model are represented, together with a red diagonal line indicating the value at which both values coincide. The dispersion for this model is high, as there is a considerable difference between the model-predicted values and the actual EEF values for each image, but it serves as a precedent for designing a network in which continuous values are obtained as network output.

Due to the fact that the value of the focusing temperature is a concrete value between −70°C and −90°C, the prediction of the best focusing temperature has to be obtained as a continuous value, so that the discrete temperature classification is not valid for the purpose described in the objectives. To overcome this, a dual regression CNN is proposed, in which a prediction of both the temperature of the images and the EEF of each of the images is obtained. To solve this problem, a double regression CNN is proposed, in which a prediction of both the temperature of the images and the EEF of each of the images is obtained.

For this purpose, the same network architecture proposed is used, in which the input of the network consists of using the images and their temperature and EEF, with a double output, one for the temperature regression and the other for the EEF regression, where the regression evaluation metrics described above are used. To obtain better results in the dispersion of the results, the

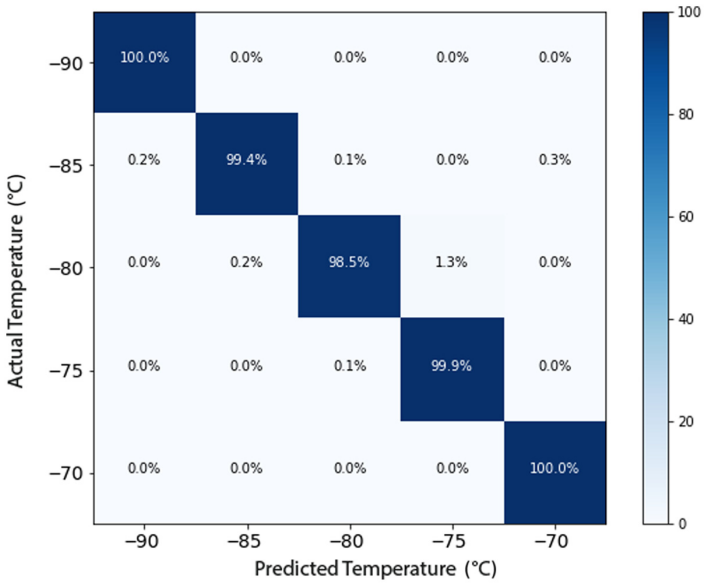

Fig. 11 Confusion matrix.

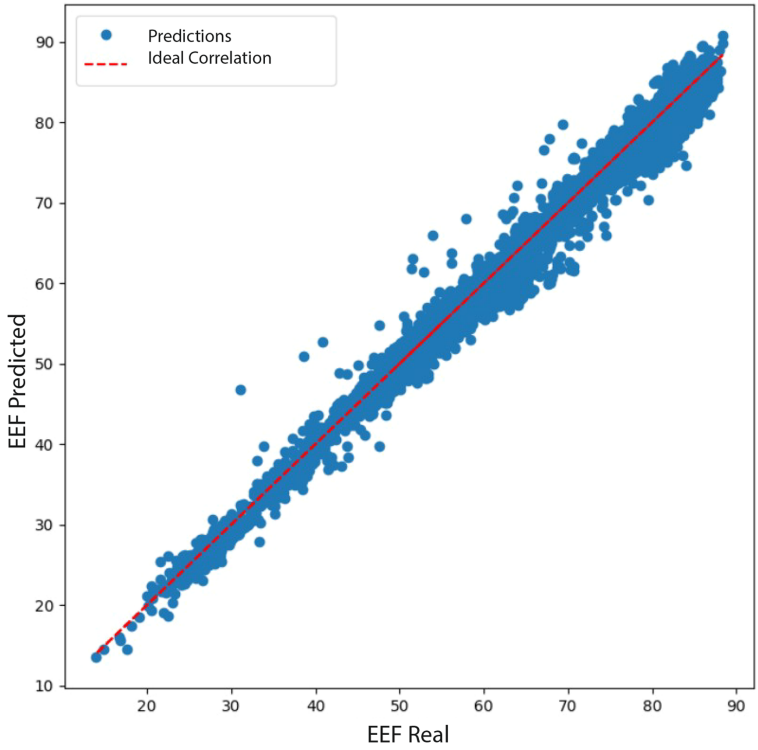

Fig. 12 Scatter plot of EEF calculation during CNN training.

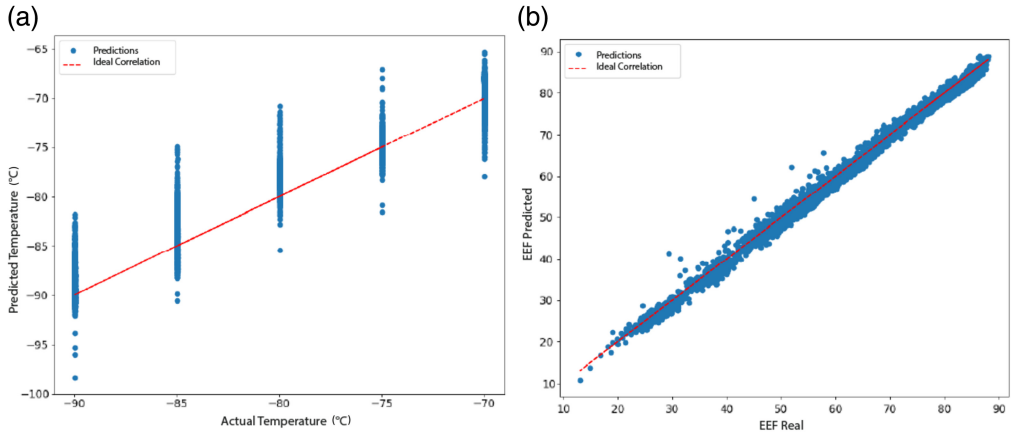

Fig. 13 Temperature regression (a) and EEF (b) for the double regression neural network model.

number of layers used in the network design is modified, increasing the size of the number of filters of the convolutional layers to 64, 128, and 256 and the size of the dense layer to 128 units.[16]

Figure 13 shows the dispersion results of the predicted and actual values of temperature and EEF when unifying the CNNs. It can be seen that the temperature prediction has a dispersion of ± 5°C for each temperature plateau and a value of $R^2 = 0.92$. In contrast, the EEF fits with a low dispersion to the red diagonal of ideal correlation, indicating that the model has improved dispersion metrics and has a good predictive ability.

3.4 CNN Implementation

Once the structure of the CNN has been defined and the parameters for an accurate classification of the results have been set, we proceed to establish the logic that allows us to obtain the best focus temperature from the images taken during the plateaux.

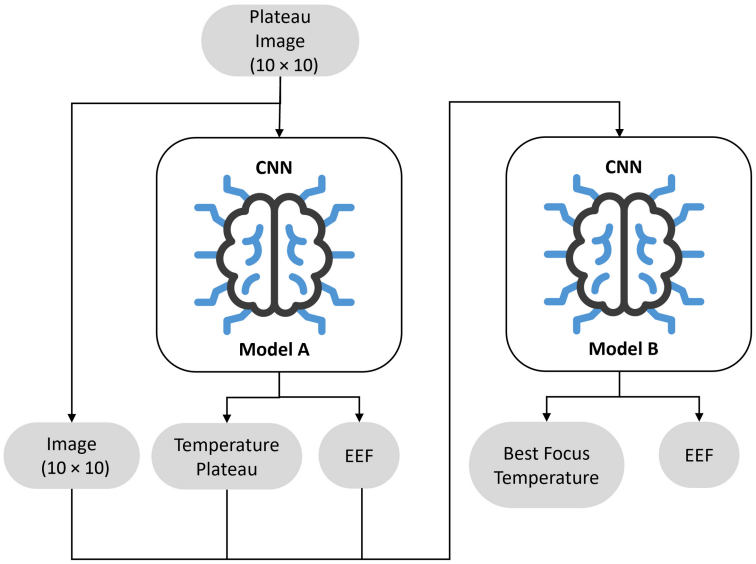

Fig. 14 Proposed neural network architecture.

To achieve the objective of temperature prediction, we propose the creation of two CNNs with the same architecture developed in the previous section: the first one (model A) will be trained with the images from the temperature plateaux, and the second one (model B) will be trained with the best focus images provided during the tests. Thus, for training, model A will use as input data the images from the plateaux, with the labels of the image temperature and EEF, obtaining a prediction on the temperature and EEF. For the training of model B, we proceed in a similar way, but using the images labeled with the data obtained at the best focus temperature.

The functioning of the network is based on two stages, Fig. 14. In the first stage, images of the temperature plateaux are input to model A to obtain preliminary temperature predictions and the EEF of the image. In the second stage, both the original image and the temperature prediction and EEF obtained in model A are used as input to model B. As model B has been trained only with best focus images, it provides the best focus temperature prediction for each of the plateau images processed in model A.

In this way, the best focus temperature is obtained as a probability distribution with each of the predictions made by the CNN, the median of this distribution being the expected temperature prediction for the particular model.

4 Results

EM, FM3, FM6, and FM10 models focusing temperatures have been predicted. For this purpose, the test images of each model are processed through model A of the CNN. The temperature and EEF output of the images are used as input for model B, together with the images. As a result of iterating the images with both models, a prediction of focus temperature and EEF is given per image, resulting in a distribution of predictions.

To determine the best focus temperature for each model, the probability distribution is plotted, and the median, which corresponds to the central value of the predictions, is calculated. The median is used because it is a more robust measure of the central value of the distribution, especially in the presence of outliers and asymmetric distributions.

The distribution of the predictions made for each model is presented below, together with the results obtained for the determination of the best focus temperature for each of them. Each of the graphs represents the distribution of predictions made on each of the images processed by the CNN. In the visualization, the median is represented by a solid line, together with a shaded area representing the interquartile range. The dashed orange line indicates the limit of the outliers, which has been calculated using the standard outlier method. This method is based on the

interquartile range, which considers as outliers values that are 1.5 times above the third quartile ($Q3$) or 1.5 times below the first quartile ($Q1$).

4.1 EM Model

A total of 3690 images are used for the prediction of this model, and the distribution of predictions is shown in Fig. 15.

In this model, the median value, −74.6°C, is ∼1°C away from the mean value, −73.8°C, indicating an asymmetry in the distribution of predictions. In this case, a range can be determined for the outliers up to −68.3°C and from −79.8°C. Within this range, a significant number of predictions above the upper limit can be seen, whereas for temperatures below the lower limit, a smaller number of predictions can be observed, but with more dispersed values, also indicating an uneven distribution in the temperature predictions.

During the tests performed, some anomalies have been detected due to the existence of pixels with manufacturing defects that cause an over-registration of energy in these pixels. These anomalies can be observed in the determination of the EEF for certain field positions, which can affect the correct operation of the values. Even with these values, the best approximation temperature for the EM model is determined to be −74.6°C.

4.2 FM3 Model

The same method is used to predict the focusing temperature of the FM3 model. Figure 16 shows the distribution of the best focus temperature prediction for this model. It can be seen that the temperature prediction has a dispersion of ±5°C for each temperature plateau and a value of $R^2 = 0.92$.

The median of the temperature predictions is −76.6°C, which coincides with the mean value, indicating that the distribution is centered on this value. The interquartile range of the distribution is also determined, in which 50% of the central predictions are concentrated, the range of which is 2.2°C. The lower and upper limits of the outliers indicate the values above which the predictions of our model can be considered atypical, corresponding to temperatures of −80.9°C and −72.2°C, respectively. Therefore, the best focus temperature for this model is set at −76.6°C.

4.3 FM6 Model

A total of 2952 test images are used for the FM6 model's best focus temperature prediction. The lower number of images used in the prediction of this model is due to a lower number of images available because of the lack of a temperature plateau during the ground tests. Figure 17 shows the best focus temperature distribution obtained with the CNN prediction.

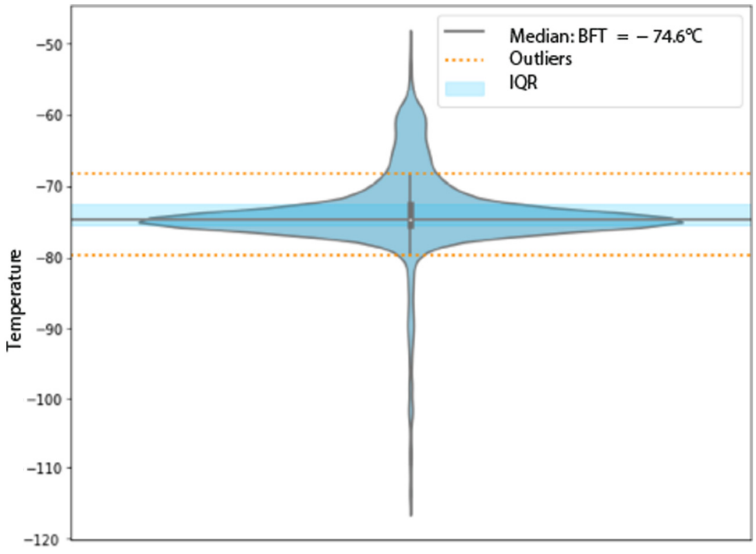

Fig. 15 Distribution of temperature predictions for the EM model.

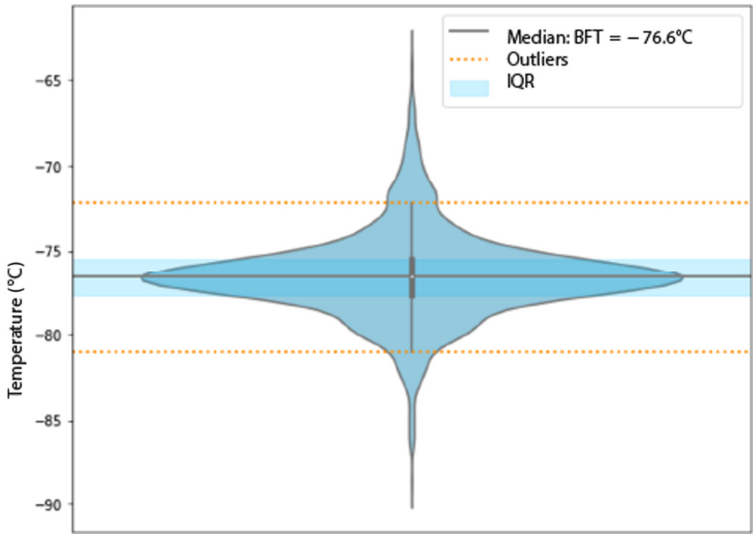

Fig. 16 Distribution of temperature predictions for the FM3 model.

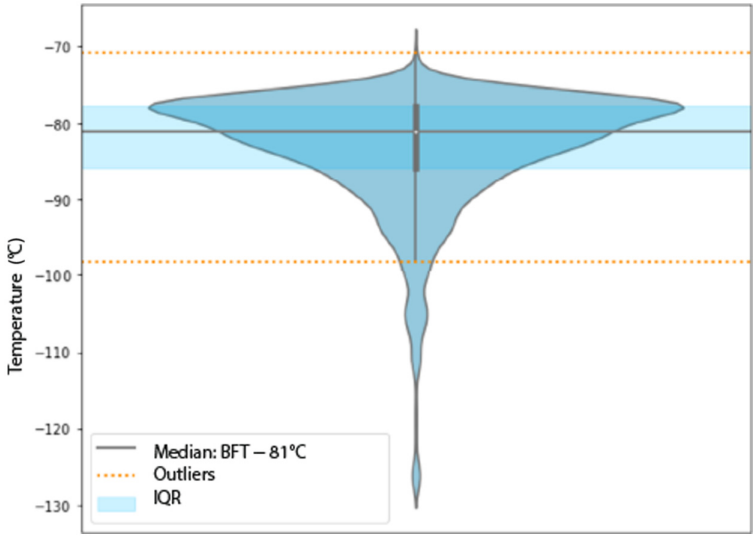

Fig. 17 Distribution of temperature predictions for the FM6 model.

In this distribution, the mean of the predictions is −83.2°C, and the median is around −81.0°C. This difference in values may be conditioned by the presence of extreme outliers that affect the distribution. Looking at the outliers, the range extends from −70.9°C to −98.0°C, indicating a wide temperature prediction, with a significant presence of outliers, the presence of outliers being higher for lower temperatures. In contrast, the interquartile range of ∼8.1°C indicates central dispersion with moderate variability in the predicted temperatures in this region.

The analysis of the model results indicates the presence of anomalies in the images used in the prediction model. In this model, there are anomalies in the EEF measurement of the images in one of the CCDs, which can distort the accuracy of the temperature predictions. Figure 18 shows the EEF of one of the plateau at −70°C where a FOV with high levels of EEF can be observed.

Despite the presence of anomalies in the images used for the prediction of this model due to manufacturing defects, the best focus temperature of this model can be determined with high reliability. With these results, it can be determined that the best focus temperature of the FM6 model is −81.0°C.

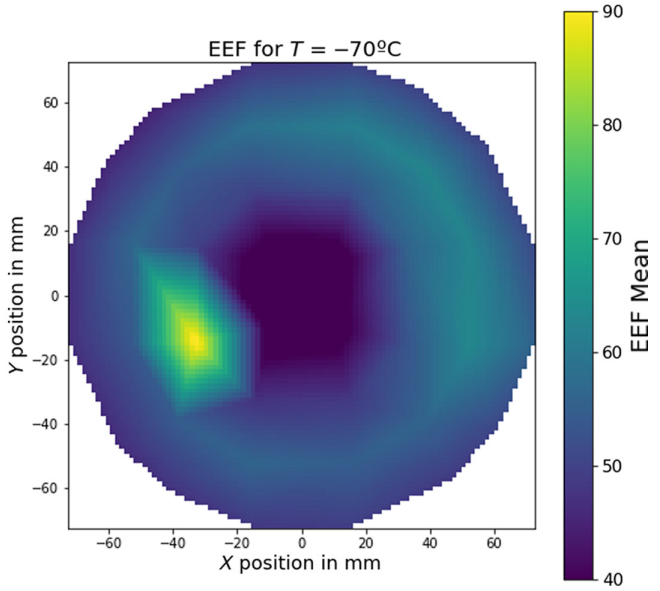

Fig. 18 Visible manufacturing anomalies on the FM6 EEF at the temperature of −70°C.

4.4 FM10 Model

To check that there is no overfitting in the CNN and that the network has learned to predict the best focus temperature and not the one learned from the models used for its training, images of a model that has not been used to train the neural network are introduced. For the prediction of the focus temperature of the FM10 model (Fig. 19), a total of 3690 images corresponding to the 5 temperature plateaux performed in the functional tests are used.

The results of this model show a considerable discrepancy between the mean and median predictions. Although the mean is at the temperature of −85.6℃, the median is at −81.1℃. This difference suggests a skewed distribution toward lower temperature values, influenced by the presence of outliers. The dispersion of the data is high, with a variance value of 190℃ and a standard deviation of 13.8℃. These values indicate the presence of high variability in the prediction results, which can be attributed to the presence of outliers. In the analysis of the EEF distribution on the detection surface of the CCDs of this model, the anomalies in the energy distribution can be seen that explain the presence of these anomalous temperatures in the prediction. The temperature range in the predictions is 120℃ difference between the maximum and

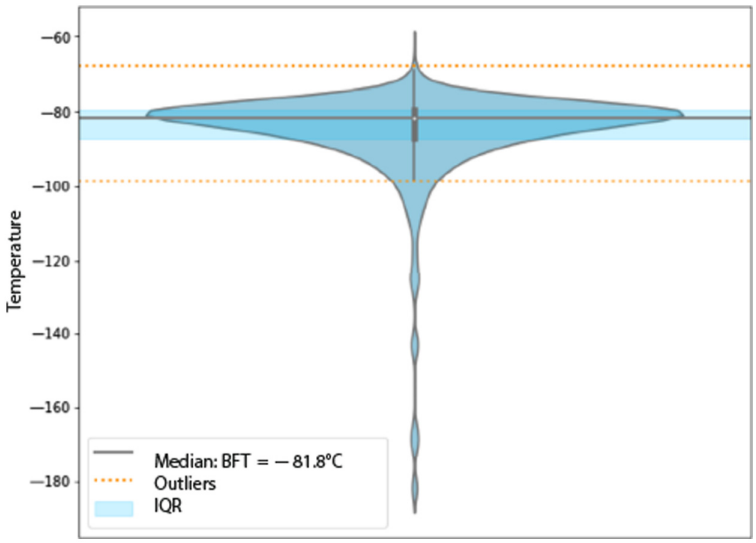

Fig. 19 Distribution of temperature predictions for the FM10 model.

Table 2 Statistical values of the predictions made by CNN of the different models evaluated.

Model	Mean (°C)	Median (°C)	SD	Kurtosis	Variance
FM3	−76.1	−75.7	2	−0.9	2.9
FM6	−83.0	−83.2	8	6.8	60.8
FM10	−85.8	−81.8	14	22.1	190.1
EM	−73.7	−74.6	6	10.4	33.86

minimum values; however, the interquartile range of 7.7°C indicates that 50% of the predictions are around the median value, which is a narrower range. These results indicate that the temperature prediction is concentrated, with high probability, around the median, but the presence of outliers contributes considerably to the dispersion of the data.

With these results, the best focus temperature of the FM10 model is set at −81.1°C.

Table 2 summarizes the statistical values obtained with the results of the best focus temperature prediction using CNN.

The following conclusions can be drawn from the values of the statistical study of each model:

- The central tendency calculations, both the mean and the median, are very close in all the models, suggesting that the data may not be skewed, resulting in a balanced distribution around the mean. In the model where these measurements differ the most are in models FM6 and FM10, where the presence of extreme outliers in the lowest temperatures can be seen in the distribution.
- The variance is a measure of the total scatter of the data. Variance-high values at EM, FM6, and FM10 is suggesting a large variability in the temperatures predicted in these models compared with those predicted for the FM3 model. This may be due to the presence of outliers in the EEF of the images corresponding to specific field positions, identified with defects in the manufacturing of the CCDs.
- Kurtosis is a measure of shape that indicates how flattened or steeped a distribution is. The positive value of kurtosis in the FM6, FM10, and EM models suggests narrower distributions compared with FM3, indicating that the predictions are more concentrated around the mean and a higher certainty in the predictions.
- The evaluation of the dispersion through the standard deviation (SD) indicates a higher variability of the predictions for the models with higher values, such as FM6, FM10, and EM, compared with the FM3 model. This measure reinforces the assertion of the influence of outliers in the calculation of the best focus temperature.

4.5 Model Comparison

To determine the quality of the CNN model developed in this work, the results obtained by both methods are compared. In addition to the results of the descriptive analysis of each model, the data of the best focus temperatures obtained by both methods of determination, statistical prediction, and CNN prediction are summarized in Fig. 20. In this visualization, the results obtained with both methods are represented in a box plot. This type of representation is particularly useful for comparing the central tendency and variability of the data, as it provides a clear visualization of the interquartile range (IQR), which covers 50% of the central data. The lower and upper limits of the box represent the first and third quartiles ($Q1$ and $Q3$), respectively, and the lines inside the box indicate the median of the data. Points outside the box, corresponding to outliers, are shown individually, highlighting the presence of extreme values in the predictions.

It can be seen that the values obtained by both methods present similar results, as evidenced by the fact that the values obtained by each method are within the corresponding interquartile ranges. This suggests that both methods are providing compatible estimations of the best focus temperature. However, a closer examination reveals differences in the dispersion of the results. The statistical prediction method shows a smaller dispersion, as indicated by narrower IQRs, which suggests that the predictions are more consistent and less influenced by extreme values.

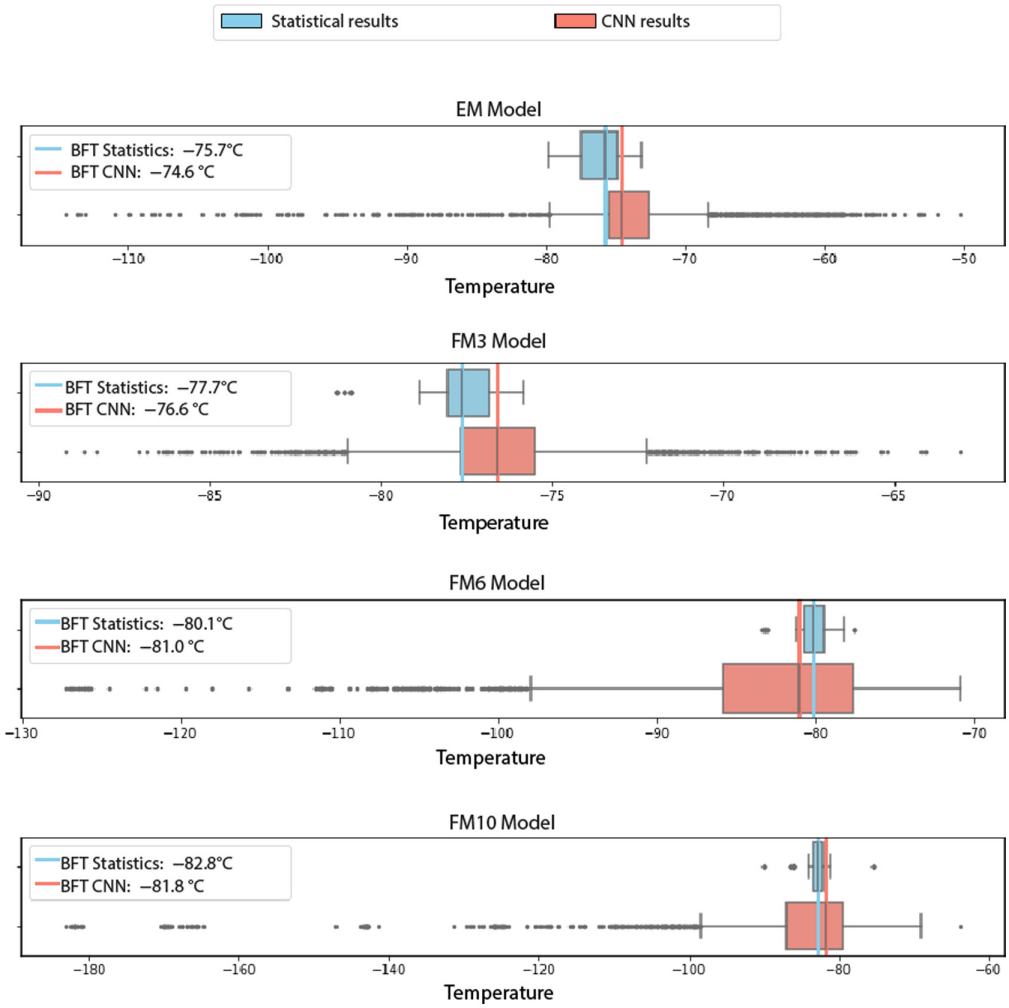

Fig. 20 Graphical comparison of statistical results and CNN predictions of BFT using box plots for each model.

In contrast, the CNN predictions exhibit a higher number of outliers and a wider dispersion, which may be attributed to the sensitivity of the neural network to anomalies in the input data, such as manufacturing defects in the CCDs or noise in the images.

Despite these challenges, the CNN predictions demonstrate a strong potential for accurately estimating the best focus temperature, as the median values of the predictions are generally close to those obtained through statistical methods. This indicates that the CNN is capable of capturing the underlying patterns in the data, even in the presence of noise and anomalies. The ability of the CNN to process large volumes of data and provide predictions in a fraction of the time required for statistical methods makes it a valuable tool for this application.

Comparing the results obtained using both methods, we can observe considerable differences in the accuracy obtained for some models. Even taking into account the standard deviation of the results obtained, the differences in the temperature values predicted by the method proposed using CNN compared with the statistical determination do not differ by more than 1°C. Considering that the statistical method requires the complete characterization of the cameras in each of the plateaux to determine the BFT, the CNN-based method provides a reasonable prediction of the BFT by analyzing data from a smaller number of plateaux. This significantly reduces the amount of data and operational time required.

In summary, although the statistical method provides more bounded and consistent results, the CNN offers a promising alternative with the potential for further improvement. By addressing the issues related to outliers and dispersion, the CNN could become a robust and efficient method for determining the best focus temperature, paving the way for its application in the calibration and operation of space telescopes such as PLATO.

5 Conclusion

In this work, we propose an alternative method for the determination of the focusing temperature of the PLATO space telescope flight models using convolutional neural networks. By implementing this system, the determination of the best focus temperature of each model is achieved in accordance with the statistical results.

One of the main requirements for the determination of the best focus temperature is that it needs to be known to within ± 3°C of accuracy in the ground characterization. This temperature will be determined with a higher degree of accuracy in the on-orbit re-calibration as part of the mission commissioning. Therefore, as can be seen from the accuracy obtained by the predictions made with the CNN model, the temperature value together with its uncertainty meets the requirement. In this way, a method is established which, despite the existence of defects in the manufacture of the electronic detection devices of the instrumentation, is capable of establishing the best focus temperature.

For a mission with a large number of cameras, such as PLATO, this reduction in the required number of measurements translates into a significant decrease in operational time, making the CNN-based approach considerably faster and more efficient from an operational perspective. Consequently, the results obtained by the method proposed in this work indicate the feasibility of implementing a flight instrument calibration system under operational space conditions, both during ground-based testing campaigns and during the orbital calibration phase throughout the instrument's operational lifetime.

To improve the performance of the neural network, it is suggested that a number of actions can be implemented to improve the accuracy of the predictions and reduce the uncertainty associated with the results, including the following: First, the training process can be improved by preprocessing the images with anomalies in the affected CCDs. As the network has been trained using images with unexpected behavior due to manufacturing defects, it is essential to preprocess these images by removing them from the training set. This would enhance the quality of the dataset and allow the CNN to better learn the patterns and representative features of the telescope's focusing system, ultimately improving the accuracy of the predictions. This action allows the CNN to learn patterns and representative features of the telescope's focusing system, allowing the network to better identify and generalize significant features of the system, thus improving the accuracy of the predictions.

In addition, expanding the diversity of the images used for training can further improve the neural network's performance. For the training of the neural network, only images with discrete temperatures corresponding to the five temperature plateaux have been used. In the transient region, images with a continuous range of temperatures are identified, which allows the network to identify images with a continuous range of temperatures. Exploring the definition of the network by imaging all regions of the test allows for increased variability of the training samples. This implementation is expected to improve the accuracy of the predictions to optimize the characterization processes of the cameras.

Finally, exploring new architectures can significantly enhance both accuracy metrics and training losses. It is recommended to experiment with different architectures by altering the topology and examining the impact of different activation functions on the results. In addition, implementing regulators that allow the adjustment of evaluation metrics or the tuning of hyperparameters can correct potential imbalances in the model, further optimizing its ability to generalize.

By implementing these actions in the proposed CNN, it is intended to obtain a better accuracy in the determination of the focusing temperature, allowing to reduce the dispersion of the predictions, providing a rigorous method for the calibration of the best focusing temperature of the space telescopes of the PLATO mission.

Disclosures

The authors declare there are no financial interests, commercial affiliations, or other potential conflicts of interest that have influenced the objectivity of this research or the writing of this paper.

Acknowledgments

Authors would like to thank to Agencia Estatal de Investigación of Ministerio de Ciencia, Innovación y Universidades of Spain for the MICIU/AEI/10.13039/501100011033 and ERDF/EU grants PID2019-107061GB-C61/C62 and PID2023-147338NB-C21/C22 as well as to INTA, for the funding support to all the activities described in this paper.

This work presents results from the ESA space mission PLATO. The PLATO payload, the PLATO Ground Segment, and PLATO data processing are joint developments of ESA and the PLATO Mission Consortium (PMC). Funding for the PMC is provided at national levels, in particular by countries participating in the PLATO Multilateral Agreement (Austria, Belgium, the Czech Republic, Denmark, France, Germany, Italy, the Netherlands, Portugal, Spain, Sweden, Switzerland, Norway, and the United Kingdom) and institutions from Brazil. Members of the PLATO Consortium can be found at Ref. 17. The ESA PLATO mission website.[18] We thank the teams working for PLATO for all their work.

The authors acknowledge the use of the code available at https://github.com/Wiflys13/PLATO_CNN, which was developed for the analysis presented in this work.

Language assistance tools were used exclusively for grammatical and stylistic corrections. The scientific content, methodology, results, and conclusions are entirely original and were produced by the authors.

References

1. H. Rauer et al., "The PLATO mission," *Exp. Astron.* **59**, 26 (2024).
2. ESA, "*PLATO: revealing habitable worlds around solar-like stars, definition study report*," ESA-SCI (2017).
3. H. Rauer et al., "The PLATO mission," *Astronomische Nachrichten* **337**(8–9), 961–963 (2016).
4. K. Sooknunan et al., "Classification of multiwavelength transients with machine learning," *Mon. Not. R. Astron. Soc.* **502**(1), 206–224 (2021).
5. Y. Cheng, R. Kong, and L. Kong, *Applications of Artificial Intelligence in Astronomical Big Data*, pp. 347–375, Elsevier (2020).
6. A. Khan, "Deep learning at scale for the construction of galaxy catalogs in the dark energy survey," *Phys. Lett. B* **795**, 248–258 (2019).
7. V. Nascimbeni et al., "The PLATO field selection process. I. Identification and content of the long-pointing fields," *Astron. Astrophys.* **658**, A31 (2022).
8. M. Pertenais et al., "Overview of PLATO's cameras on-ground and in orbit calibration and characterisation," *Proc. SPIE* **11852**, 1185209 (2021).
9. E. Gecht, *Optics*, Addison-Wesley (2002).
10. R. E. Fischer, *Optical System Design*, SPIE Press, Bellingham, Washington (2008).
11. F. Montoro et al., "INTA as test house for PLATO: telescope flight model TVAC testing and calibration first results," *Proc. SPIE* **13092**, 130924T (2024).
12. E. Borreguero et al., "INTA as test house for PLATO: telescopes TVAC testing and calibration set-up preparation and EM results," *Proc. SPIE* **13092**, 130924S (2024).
13. C. M. Bishop, *Pattern Recognition and Machine Learning*, Springer (2006).
14. F. Borsa et al., "PLATO EM first cryogenic vacuum test campaign PSF results," *Proc. SPIE* **12180**, 121801D (2022).
15. C. C. Aggarwal, *Neural Networks and Deep Learning*, Springer (2023).
16. Y. LeCun et al., "Gradient-based learning applied to document recognition," *Proc IEEE* **86**(11), 2278–2324 (1998).
17. Planetary Transits and Oscillations of Stars: the ESA M3 mission in the Cosmic Vision 2015-2025 https://platomission.com/.
18. The PLATO Mission, https://www.cosmos.esa.int/plato.

Guillermo Mercant Rubio received his BSc degree in physics from Universidad Complutense de Madrid (UCM) and his MSc degree in data science and big data from Universidad Internacional de Valencia (VIU). He completed a three-year fellowship at INTA's Space Optics Department, developing components for future terahertz missions and supporting AIT activities for ESA missions such as PLATO. He currently works as an AIT engineer for ground instrumentation at the Extremely Large Telescope (ELT) in Chile.

Biographies of the other authors are not available.